Title: Identification of Rare High-Avidity, Tumor-Reactive CD8+ T Cells by Monomeric TCR-Ligand Off-Rates Measurements on Living Cells.

Authors: Hebeisen M, Schmidt J, Guillaume P, Baumgaertner P, Speiser DE, Luescher I, Rufer N

Journal: Cancer research

Year: 2015 May 15

Volume: 75

Issue: 10

Pages: 1983-91

DOI: 10.1158/0008-5472.CAN-14-3516

Identification of rare high avidity, tumor reactive CD8+ T cells by monomeric TCR-ligand off-rates measurements on living cells

Michael Hebeisen[1,*], Julien Schmidt[2,3,*], Philippe Guillaume[2,3], Petra Baumgaertner[2], Daniel E. Speiser[1,2], Immanuel Luescher[1,2,3] and Nathalie Rufer[1,2]

[1]Department of Oncology, Lausanne University Hospital Center and University of Lausanne, Lausanne, Switzerland

[2]Ludwig Center for Cancer Research, University of Lausanne, Lausanne, Switzerland

[3]TCMetrix Sàrl., 1066 Epalinges, Switzerland

[*] These authors contributed equally to this work

Corresponding author: Nathalie Rufer, PhD, MD, Department of Oncology, Lausanne University Hospital Center, Avenue Pierre-Decker 4, 1011 Lausanne, Switzerland. Phone: 0041-21-314-0199. Fax: 0041-21-314-7477. E-mail: Nathalie.Rufer@unil.ch

Running title: NTAmers predict tumor-specific T cell responses

Word counts: 5000

Keywords: human, melanoma, CD8+ T cells, tumor-specific, TCR, pMHC, reversible NTAmers, flow cytometry, monomeric off-rates, k_{off}, avidity, calcium flux, target cell killing

Abbreviations: TCR, T cell receptor; MHC, peptide-major histocompatibility complex; A2, HLA-A*0201; NTA, nitrilotriacetic acid; SPR, surface plasmon resonance; PBMC, peripheral blood mononuclear cells

AUTHOR CONTRIBUTIONS

Conception and design: M. Hebeisen, J. Schmidt, I. Luescher, N. Rufer

Development of methodology: M. Hebeisen, J. Schmidt, P. Guillaume, I Luescher, N. Rufer

Acquisition of data (provided animals, acquired and managed patients, provided facilities, etc.): M. Hebeisen, J. Schmidt, P. Baumgaertner

Analysis and interpretation of data (e.g., statistical analysis, biostatistics, computational analysis): M. Hebeisen, N Rufer

Writing, review and/or revision of the manuscript: M. Hebeisen, J. Schmidt, D.E. Speiser, I. Luescher, N. Rufer

Study supervision: N. Rufer

DISCLOSURE OF POTENTIAL CONFLICTS OF INTEREST

No potential conflicts of interest were disclosed.

ABSTRACT

The avidity of the T cell receptor (TCR) for antigenic peptides presented by the major histocompatibility complex (pMHC) on cells is a key parameter for cell-mediated immunity. Yet a fundamental feature of most tumor antigen-specific CD8+ T cells is that this avidity is low. In this study, we addressed the need to identify and select tumor-specific CD8+ T cells of highest avidity, which are of the greatest interest for adoptive cell therapy in cancer patients. To identify these rare cells, we developed a peptide-MHC multimer technology, which uses reversible Ni^{2+}-nitrilotriacetic acid histidine tags (NTAmers). NTAmers are highly stable but upon imidazole addition they decay rapidly to pMHC monomers, allowing flow cytometry-based measurements of monomeric TCR-pMHC dissociation rates of living CD8+ T cells on a wide avidity spectrum. We documented strong correlations between NTAmer kinetic results and those obtained by surface plasmon resonance (SPR). Using NTAmers that were deficient for CD8 binding to pMHC, we found that CD8 itself stabilized the TCR-pMHC complex, prolonging the dissociation half-life several-fold. Notably, our NTAmer technology accurately predicted the function of large panels of tumor-specific T cells that were isolated prospectively from cancer patients. Overall, our results demonstrated that NTAmers are effective tools to isolate rare high-avidity cytotoxic T cells from patients for use in adoptive therapies for cancer treatment.

INTRODUCTION

Binding of TCR to peptide-MHC (pMHC) complex is the key step for T cell activation and cellular immune responses (1). Efficient triggering of T cell responses critically depends on the strength of TCR-mediated antigen recognition, namely it has been shown that strong binding to pMHC confers superior effector function than weak interactions (2-7). This is of particular interest for immunotherapy based on adoptive T cell transfer, aiming to convey immune reactivity against tumor-associated antigens, for which endogenous T cell responses are usually weak. Many tumor antigens are in fact self-antigens that are expressed in the thymus, and accordingly, most tumor-reactive T cells of high avidity become negatively selected, in contrast to pathogen-specific T cells (8). Therefore, there is a need for a robust technology that allows rapid identification and isolation of CD8+ T cells expressing TCRs capable to efficiently activate and enhance T cell function against malignant cells.

TCR-pMHC binding parameters are typically assessed by SPR, which requires laborious and expensive production of soluble TCRs and ignores the TCR-pMHC avidity effects related to CD8 co-receptor binding. On the other hand, kinetic measurements using pMHC tetramers or multimers have been extensively studied on the surface of antigen-specific CD8+ T cells, but due to the multivalent and heterogeneous composition of these multimers, this approach does not allow to accurately determine TCR-pMHC dissociation rates (9). Binding and dissociation measurements should ideally be performed using monomeric pMHC complexes. Because TCR-pMHC interactions typically exhibit weak affinities and fast dissociation rates, this has long precluded conclusive measurements with monomeric pMHCs (10).

Nauerth et al. (11) recently measured monomeric TCR-pMHC dissociation kinetics using reversible *Strep*tamers and reported that virus-specific CD8+ T cells with longer half-lives (low

k_{off} rates) conferred increased functional avidity and better *in vivo* protection than T cells exhibiting shorter $t_{1/2}$ (high k_{off} rates). However, the *Strep*tamer assay (11) needs a significant lag time until monomeric TCR-pMHC dissociation starts to become detectable, limiting thereby off-rate analyses to antigen-specific T cells of relative long half-lives, typically found in immune responses against pathogens. Moreover, accurate measurements of TCR-pMHC binding parameters on living T cells (11-14) require specialized equipment, which is currently not available for the high-throughput screen of antigen-specific T cell populations.

To overcome these limitations, we here applied pMHC multimers built on reversible chelate complexes of Ni^{2+}-nitriloacetic acid (NTA) with oligohistidines (15) allowing the efficient and direct cytometry-based assessment of monomeric TCR-pMHC dissociation kinetics on the surface of (self) tumor-specific CD8+ T cells. We found that the NTAmer technology accurately predicted T cell biological responses within a large panel of tumor-specific T cell clones, providing novel means for the direct isolation of rare functionally relevant CD8+ T cells for adoptive cell transfer therapy.

MATERIALS AND METHODS

Ethics statement

The three HLA-A*0201-positive patients had stage III/IV metastatic melanoma and were included in immunotherapy studies (patient LAU 50, NCT00112242; patient LAU 155, NCT00002669; and patient LAU 618, NCT00112229; www.clinicaltrials.gov). The studies were designed and conducted according to the relevant regulatory standards, upon approval by the ethical commissions and regulatory agency of Switzerland. Patient recruitment, study procedures, and blood withdrawal were done upon written informed consent.

Primary bulk CD8+ T cells and generation of tumor-specific CD8+ T cell clones

Human primary HLA-A*0201^{pos} CD8+ T lymphocytes were obtained following positive enrichment using anti-CD8-coated magnetic microbeads (Miltenyi Biotec), and cultured in RPMI supplemented with 8% human serum (HS) and 150 U/ml recombinant human IL-2. HLA-A*0201-NTAmer^{pos} (NY-ESO-1$_{157-165}$ -specific or Melan-A^{MART-1}-$_{26-35}$ -specific) T cells from melanoma patient LAU 50 and LAU 618, respectively, were sorted by flow cytometry, cloned by limiting dilution and expanded in RPMI 1640 medium supplemented with 8% HS, 150 U/ml recombinant human IL-2, 1 μg/ml phytohemagglutinin (PHA) (Oxoid) and irradiated (30 Gy) allogeneic PBMCs as feeder cells. For patient LAU 155, twenty HLA-A*0201/NY-ESO-1$_{157-165}$ -specific T cell clones expressing dominant TCR BV1, BV8 and BV13 clonotypes and a non-dominant TCR BV2 clonotype were selected from our previously generated database of T cell clones (16), thawed and *in vitro* expanded before further use. Primary bulk CD8+ T cells and tumor-specific T cell clones were expanded by periodic restimulation with 30-Gy irradiated allogeneic PBMCs and 1 μg/ml PHA.

Lentiviral production and cell transduction

Full-length codon-optimized TCR AV23.1 and TCR BV13.1 chain sequences of a dominant HLA-A*0201/NY-ESO-$1_{157–165}$ specific T cell clone of patient LAU 155 (16) were cloned in the pRRL third generation lentiviral vectors as an hPGK-AV23.1-IRES-BV13.1 construct and structure-based amino acid substitutions were introduced into the WT TCR sequence as described previously (5). Lentiviral production was performed using the calcium-phosphate method and concentrated supernatant of lentiviral-transfected 293T cells was used to infect TCR-α knockout CD8+ SUP-T1 cells (ATCC number CRL-1942, mycoplasma-free), CD8-null Jurkat T cells (ATCC number TIB-152; mycoplasma-free), or primary CD8+ T cells overnight. Levels of transduced TCR expression on SUP-T1, Jurkat cells and primary bulk CD8+ T cells were monitored with PE-labeled HLA-A*0201/NY-ESO-$1_{157-165}$ specific multimers (TCMetrix Sàrl) and FITC-conjugated BV13.1 antibody (Beckman Coulter).

NTAmer production and staining

NTAmers were synthetized by TCMetrix Sàrl (www.tcmetrix.ch) as described in (15). NTAmers are composed of Streptavidin-Phycoerythrin (SA-PE, Invitrogen) complexed with biotinylated peptides carrying four Ni^{2+}-nitrilotriacetic acid (NTA_4) moieties and non-covalently bound to His-tagged HLA-A*0201 monomers containing β2m or a Cy5-labeled β2m. Monomers were obtained by refolding of the HLA-A*0201 heavy chain in the presence of β2m or Cy5-labeled β2m containing the S88C mutation with Cy-5-maleimide (GE Healthcare) and the analog NY-ESO-$1_{157-165}$ [SLLMWITQA] or Melan-$A^{MART-1}{}_{26-35}$ [ELAGIGILTV] tumor antigenic peptide, optimized for enhanced HLA-A*0201 binding. After purification on a Superdex S75 column, pMHC monomers were mixed at a 10-fold ratio with SA-PE-NTA_4 in the presence of Ni^{2+} as described in (15). The same procedure was used to prepare CD8-binding deficient HLA-A*0201 monomers bearing the

D227K/T228A mutations in the HLA-α3 domain (17). Dually labeled NTAmers containing SA-PE and Cy5-labeled monomers were used for dissociation kinetic measurements as described below. Single labeled NTAmers containing SA-PE and unlabeled monomers were used for flow cytometry-based sorting of tumor-specific T cells. Once sorted, tumor-specific T cells were treated with 100 mM imidazole at 4°C, allowing the rapid dissociation of the SA-PE-NTA_4 scaffold and pMHC monomers before *in vitro* T cell cloning by limiting dilution.

Dissociation kinetic measurements

TCR-transduced CD8+ SUP-T1 or CD8- Jurkat cells ($5x10^5$ cells) and tumor-specific CD8+ T cell clones ($2x10^5$ cells) derived from patients LAU 155, LAU 50 and LAU 618 were incubated for 40 min at 4°C with HLA-A*0201/NY-ESO-$1_{157-165}$ or HLA-A*0201/ Melan-$A^{MART\text{-}1}{}_{26-35}$ NTAmers containing streptavidin (SA)-phycoerythrin (PE) and Cy5-labeled monomers in 50 µl FACS buffer (PBS supplemented with 0.5% BSA, 15 mM HEPES and 0.02% NaN_3). After a washing step, cells were suspended in 500 µl FACS buffer at 15°C (for SUP-T1 and Jurkat cells) or 200 µl FACS buffer at 4°C (for primary T cell clones from melanoma patients) and cell surface-associated mean fluorescence was measured under constant temperature using a thermostat device (15°C for SUP-T1 and Jurkat cells and 4°C for primary T cell clones) on a SORP-LSR II flow cytometer (BD Biosciences) following gating on living cells. PE-NTA_4 and Cy5-pMHC monomer fluorescence was measured before (between 30s to 1 min; baseline) and during 5 to 10 minutes after the addition of imidazole (100 mM). High-resolution microscopy flow analysis was performed on an Amnis ImageStream^x Mark II instrument (Merck Millipore) using a 40x objective. Staining was performed as described above for SUP-T1 cells. PE-NTA_4 and Cy5-pMHC monomer fluorescence was measured before (t = 0) and during 5 minutes upon the addition of imidazole (100 mM) at 20°C. A

60 seconds lag time due to the automated handling of cell suspension by the Amnis instrument precluded earlier time-point measurements.

Dissociation kinetic data analysis

Flow cytometry-based data were processed using the FlowJo software (v.9.6, Tree Star, Inc.). After gating on living cells, PE or Cy5 mean fluorescence intensity was derived using the kinetic module of the FlowJo software. Gates of 6 seconds period were created following addition of imidazole at the following time-points; 15s, 30s, 45s, 60s, 90s, 120s and then every minute for 10 minutes. Geometric MFI was measured at each time-points after gating on HLA-A*0201/NY-ESO-$1_{157\text{-}165}$- or HLA-A*0201/ Melan-$A^{MART\text{-}1}{}_{26\text{-}35}$-specific staining. Irrelevant Flu-specific gMFI values were systematically subtracted at the various time-points. Corrected gMFI values were plotted and analyzed using the GraphPad Prism software (v.6, GraphPad).

Calcium mobilization assays

5×10^4 TCR- transduced SUP-T1 or primary bulk CD8+ T cells were loaded with 2 μM Indo 1-AM (Sigma-Aldrich, Switzerland) for 45 minutes at 37°C. Cells were washed and resuspended in 250 μl pre-warmed RPMI containing 2% FCS. Baseline was recorded for 30 seconds before 1 μg/ml of undissociated HLA-A*0201/NY-ESO-$1_{157\text{-}165}$ NTAmers (for SUP-T1) or 1 μg/ml HLA-A*0201/NY-ESO-$1_{157\text{-}165}$-specific multimers (for primary CD8+ T cells) were added to the cells allowing specific stimulation. Intracellular Ca^{2+} flux was assessed over 5 minutes under UV excitation and constant temperature of 37°C using a thermostat device on a LSR II SORP (BD Biosciences) flow cytometer. Indo-1 (violet)/Indo-1 (blue) 405/525 nm emission ratio was analyzed by FlowJo kinetics module software (TreeStar).

Chromium release and tumor recognition assays

The functional avidity of antigen recognition was analyzed in a 4-hour ^{51}Cr-release assay using TAP$^{-/-}$ deficient T2 (HLA-A*0201^{pos}) target cells pulsed with serial dilutions of the natural NY–ESO-1$_{157-165}$ peptide [SLLMWITQC] for tumor-specific T cell clones derived from patient LAU 155 and LAU 50 or the natural Melan-A$^{MART-1}{}_{26-35}$ peptide [EAAGIGILTV] for tumor-specific T cell clones derived from patient LAU 618. The NY-ESO-1 peptide was preincubated for 1 hour at room temperature with the disulfide-reducing agent Tris [2-carboxyethyl] phosphine (TCEP; 2 mM, Pierce Biotechnology) before functional assays. The percentage of specific lysis was calculated as follows: 100 × (experimental − spontaneous release)/ (total − spontaneous release). For T cell clones of defined TCR αβ clonotypes previously derived from patient LAU 155 (16), antigen-specific recognition and lytic activity was further assessed against the melanoma cell lines Me 275 (HLA-A2^{pos}/NY-ESO-1^{pos}) and NA8 (HLA-A2^{pos}/NY-ESO-1^{neg}).

Statistics

Statistical analyses were done with the GraphPad Prism software. A minimum of three independent experiments were performed to ensure a statistical power of 100% at $\alpha = 0.05$ (Fig. 2 and 3), and a sample size ≥ 23 to ensure a statistical power of 80% at $\alpha = 0.05$ (Fig. 5). Correlation analyses were performed using Pearson (Fig. 2 to 4) or Spearman (Fig. 5) coefficient r. The associated p value (two-tailed, $\alpha = 0.05$) quantifies the likelihood that the correlation is due to random sampling. Two different investigators performed each TCR-pMHC dissociation kinetic experiment independently, and experiments described in Figure 5 were performed blinded for both sample allocation and outcome assessment.

RESULTS

Direct measurements of monomeric TCR-pMHC dissociation kinetics by NTAmers

We previously developed a method for the isolation and analysis of antigen-specific cytotoxic T cells by reversible NTAmers (10, 15). Upon addition of imidazole at low, non-toxic concentration, the SA-PE-NTA_4 moieties rapidly decay (average dissociation half-life of 2.5 sec), thereby releasing the pMHC monomers bound at the cell surface. Consequently, NTAmers allow FACS-sorting of CD8+ T cells without inducing adverse effects on the cell integrity (e.g. activation-induced cell death) (10, 15). Taking advantage of the fact that NTAmers can be switched from stable binding to rapid dissociation, a two-color NTAmer was engineered to assess monomeric TCR-pMHC dissociation kinetics directly on living CD8+ T cells (Fig. 1A). We first evaluated this novel approach by direct visualization of the dissociation process on individual human CD8+ SUP-T1 cells expressing TCRs of increasing affinities for the HLA-A*0201-restricted tumor epitope NY-ESO-$1_{157\text{-}165}$ (18), using a flow cytometer generating simultaneous high resolution microscopy imaging (ImageStream^X MarkII) (Fig. 1B). As predicted, we observed strongest and most sustained fluorescence levels for T cells of very high TCR affinities (e.g. QMα and wtc51m). Because of a 60 sec lag time due to the automated handling of cells following the addition of imidazole, the imaging approach precluded the visualization of labeled monomeric pMHC dissociation for T cells expressing TCRs ranging within the physiological range (e.g. V49I, wild-type and DMβ). To solve this issue, we used a conventional flow cytometer (LSRII-SORP) equipped with a thermostat, which drastically reduced the lagging time to less than 5 sec (Fig. 1C), thereby allowing the accurate assessment of monomeric pMHC dissociation kinetics on the surface of CD8+ T cells across a wide TCR affinity spectrum (Fig. 1D, Supplementary Fig. S1A). To validate the NTAmer technology, we

next compared these dissociation values with SPR kinetics data obtained with the corresponding soluble TCRs (Table 1). Robust correlations were found between NTAmer-based cell surface monomeric pMHC dissociation kinetics (half-live $t_{1/2}$ and k_{off}), with both k_{off} rates and affinities measured by SPR, contrasting with the weaker correlations obtained with pMHC tetramers (Fig. 2A, Supplementary Fig. S2A).

CD8 co-receptor stabilized the TCR-pMHC complex by prolonging the dissociation half-life by a factor of 3 to 4-fold

To precisely quantify the contribution of CD8 co-receptor to monomeric TCR-pMHC dissociation, we generated NTAmer$^{227\text{-}228}$ variants containing the HLA-A*0201 D227K/T228A mutations in the MHC α3 domain that abolish CD8 binding to pMHC (17). Using the same panel of TCR transduced CD8+ SUP-T1 cells we show that abrogating CD8-MHC binding drastically diminished dissociation half-lives ($t_{1/2}$) over the whole spectrum of TCR affinities (Fig. 2B, Supplementary Fig. S1B and C). Monomeric off-rate (k_{off} and $t_{1/2}$) correlations between NTAmers$^{227\text{-}228}$ and SPR were highly significant (Fig. 2A, Supplementary Fig. S2A). Comparison between wild-type and CD8-binding deficient NTAmer-based half-lives revealed that CD8 stabilized by a factor of 3 to 4-fold the interaction between tumor-specific TCRs and HLA-A*0201/NY-ESO-1 irrespectively of the TCR affinity (Fig. 2B). A similar effect of CD8 binding to pMHC was observed when using TCR transduced Jurkat T cells that lack CD8 expression (Fig. 2C and D; Supplementary Fig. S2B) with k_{off} and $t_{1/2}$ values that were highly comparable to those found by NTAmers$^{227\text{-}228}$ or by SPR on CD8+ T cells (Table 1). Altogether, the NTAmer technology permits (i) the precise measurements of monomeric TCR-pMHC dissociation kinetics directly on living T cells expressing a wide TCR affinity range, including

those typically found within the self/tumor-specific repertoires, and (ii) the quantification of the contribution of CD8 binding on the TCR-pMHC complex stability, which is not possible in SPR measurements.

Monomeric TCR-pMHC dissociation kinetics correlate with enhanced T cell responsiveness

Next we compared k_{off} rates obtained using NTAmers and the intracellular calcium mobilization on CD8+ SUP-T1 cells (Fig. 3A and B) and primary CD8+ T cells (Fig. 3D and E) expressing the panel of affinity-optimized TCRs against NY-ESO-1 tumor antigen. In line with our previous reports (19, 20), the Ca^{2+} flux was enhanced with increasing TCR affinity, up to reaching a plateau, while further affinity increase ($K_D < 1$ μM) resulted in reduced calcium signaling. Within the physiological TCR-pMHC affinity range, however, both SUP-T1 cells and primary T cells exhibited strong correlations between dissociation rates and Ca^{2+} mobilization (Fig. 3C and F); there was an enhanced Ca^{2+} flux in T cells of longer half-lives (low k_{off}), contrasting with the reduced signaling observed in T cells of shorter $t_{1/2}$ (high k_{off}). An overall reduction in Ca^{2+} flux was observed when using mutant multimer/HLA-A*0201$^{227\text{-}228}$ for specific stimulation, but this effect was less stringent for T cells expressing very high TCR affinities (e.g. TMα, QMα and wtc51m) (Fig. 3A and B). As previously reported (20-22), these data indicate that the degree of CD8 dependence for T cell activation inversely depends on the affinity and dissociation half-life of the TCR-pMHC interaction.

We extended these observations to a clinically relevant setting, and characterized k_{off} rates and functional avidity of T cells obtained from a large set of HLA-A*0201/NY-ESO-$1_{157\text{-}165}$-specific CD8+ T cell clones expressing well-defined TCRαβ clonotypes derived from LAU 155, a

melanoma patient with long lasting anti-tumor T cell responses (16). The dissociation rates of those cytotoxic T cell clones clustered within a narrow range (Fig. 4A, Supplementary Fig. S3A), and strongly correlated with EC_{50} target cell killing (50% maximal lysis; Fig. 4C) and tumor cell recognition (Fig. 4E), with TCR clonotypes having long half-lives (low k_{off}) exhibiting increased T cell cytotoxicity (Fig. 4B and D). Conversely, NY-ESO-1-specific TCR clonotypes with short half-lives (high k_{off}) showed reduced T cell killing capacities.

Identification of rare high avidity, tumor-specific CD8+ T cells by monomeric TCR-pMHC dissociation kinetic measurements

To find out whether NTAmers allow direct identification of tumor-specific CD8+ T cells with high tumor killing capacity, we derived 147 tumor-specific T cell clones from two other melanoma patients with detectable *ex vivo* T cell responses against the HLA-A*0201 restricted tumor antigens NY-ESO-$1_{157-165}$ and Melan-$A^{MART\text{-}1}{}_{26-35}$, respectively, and screened them for monomeric dissociation rates (Fig. 5A and D; Supplementary Fig. S3B and C). Tumor-specific T cell clones were distributed according to their TCR Vβ family expression using monoclonal antibodies and k_{off} rate analyses revealed large differences in half-lives between specific TCRs (Supplementary Fig. S4). Next, we performed killing assays with 57 clones selected for relatively low or high k_{off} values (Fig. 5B and E). We observed, for both antigenic specificities, a robust correlation between off-rates and the functional avidity (EC_{50}) determined with the cytotoxicity assay (Fig. 5C and F), demonstrating that NTAmers allow reliable assessment of surface-based TCR-pMHC dissociation kinetics and rapid selection of highly potent tumor-specific T cell clones derived from different cancer patients.

DISCUSSION

Identifying antigen-specific T cells that confer efficient effector function is critical for successful adoptive cell therapy. The stability of TCR binding for the peptide-MHC complex is a key determinant for T cell activation. Several lines of evidence argue for a close relationship between cell surface dissociation kinetics (k_{off}) and functional T cell responses (5, 23-26). Yet, rapid and accurate screening methods to measure TCR-pMHC binding kinetics are still needed to isolate antigen-specific T-cells expressing TCRs of high binding avidity. Recently, we developed a novel approach combining reversible peptide-MHC multimers (NTAmers; (15)) and real-time flow cytometry (Fig. 1). Using SPR, we had previously determined the TCR-pMHC binding strength of sequence-optimized HLA-A*0201/NY-ESO-$1_{157-165}$ specific TCRs with increasing affinity of up to 150-fold from the wild-type receptor, including two outliers, a very low- and a very high-affinity TCR (5, 20). This TCR panel provides a unique model for validating monomeric TCR-pMHC dissociation kinetics at the surface of T cells by NTAmers. Here, we demonstrate that NTAmer-based off-rates (k_{off}, $t_{1/2}$) followed the same TCR-pMHC binding hierarchy than previously established (20), in excellent agreement to both binding parameters, k_{off} and the dissociation constant K_D, obtained by SPR (Fig. 2; Table 1).

Due to their switch ability i.e. high stability and rapid reversibility (< 5 sec), NTAmers allowed accurate determination of dissociation rates, even for weak TCR-pMHC interactions, i.e. fast off-rates, such as those found for (self) tumor-specific CD8+ T cell repertoires (Fig. 4). Notably, the NTAmer approach differs from the *Strep*tamer one, which is mostly limited to the detection of CD8+ T cells of high avidity such as virus-specific cells, as it requires a significant lag time (60 sec) before monomeric TCR-pMHC dissociation becomes detectable (11). Moreover, the NTAmer-based assay represents a rapid and straightforward approach for the quantitative

assessment of monomeric k_{off} rates on a large set of cloned antigen-specific CD8+ T cells derived from different patients and tumor epitopes (HLA-A*0201/NY-ESO-$1_{157-165}$ and HLA-A*0201/Melan-$A^{MART\text{-}1}{}_{26-35}$) (Fig. 5). Importantly, we demonstrate robust correlations between dissociation off-rates and the biological responses (e.g calcium flux and target cell killing) on a large panel of CD8+ T cell clones specific for two distinct tumor antigens, indicating that TCR-ligand k_{off} rate is a reliable predictor of T cell function (Fig. 3-5).

Interactions between TCRs and pMHC are usually measured by SPR or pMHC tetramer or multimer staining, which requires one binding partner in soluble form. Both approaches have caveats. Due to their incomplete dissociation and multivalent nature, accurate off-rates data from pMHC tetramer/multimer staining measurements are imprecise. Conversely, monomeric dissociation k_{off} rates measured by the NTAmer technology were within the range of seconds to minutes, spanning a broad range (2-logs), as compared to a narrow range of minutes observed when using pMHC tetramers. Moreover, SPR fails to take into account rapid rebinding of the TCR to the same pMHC, because one of the two binding partners is constantly moving in the fluid phase, which impacts on the binding kinetics. Increased k_{on} rates have been shown to allow rapid rebinding after TCR-ligand dissociation, resulting in enhanced effective dissociation half-life of the TCR-pMHC interaction (25, 27). This may explain our observation that TCR variants with faster k_{on} (e.g. TMα and QMα) showed prolonged NTAmer-based dissociation half-lives compared to soluble monomeric off-rates measured by SPR (Table 1, Supplementary Fig. S5).

The NTAmer-based approach further deviates from SPR measurements, as it provides data on living cells and includes contributions of CD8 to TCR-pMHC interactions. The CD8 co-receptor enhances antigen recognition and T cell activation by stabilizing TCR-pMHC interaction at the cell surface (28-31) and recruiting $p56^{lck}$ to TCR/CD3 complex promoting cell signaling (32, 33).

Here we demonstrate that CD8 strengthened the TCR-pMHC binding mainly by decreasing the TCR-pMHC dissociation by a factor of 3 to 4-fold (Fig. 2), as anticipated by previous tetramer dissociation assays (22, 30). Interestingly, the CD8 stabilization factor was independent of the TCR-pMHC affinity, in contrast to the CD8 dependence for T cell activation, which can be directly linked to the affinity (3, 20, 22), and allows tuning the sensitivity and specificity of T cell responses (34).

We recently provided new evidence that T cell signaling and activation are optimal within a given TCR-pMHC affinity window (20), controlled through TCR affinity-mediated regulatory molecules, involving the inhibitory receptor PD-1 and SHP-1 phosphatase (19). Furthermore, while high avidity T cells have been shown to control tumor growth, they become preferentially tolerized in the tumor microenvironment (35) or can target normal tissues expressing the cognate antigen (36, 37). Therefore, tumor-specific T cells of high avidity may not always be functionally better, and it remains to be fully determined to which degree intermediate or high avidity T cells contribute to protective immunity. In this regard, NTAmers constitute a highly valuable tool for assessing the TCR-pMHC avidity and its relation to cell activation, signaling and function in naturally- or therapeutically-induced tumor-specific T cell responses, with TCR-pMHC affinities spanning within the physiological range.

In summary, NTAmer technology enables efficient and direct interrogation of monomeric TCR-pMHC dissociation kinetics on a large set of living antigen-specific T cells by flow cytometry, and provides novel perspectives for rapid identification of rare functionally relevant tumor-reactive CD8+ T cells . Our approach may also be applicable to the analysis of other weak protein-protein interactions. Precise and wide-spread characterization of TCR-pMHC avidities will likely improve the development of T cell based immunotherapies in cancer patients.

GRANT SUPPORT

This study was supported by the Department of Oncology of the University of Lausanne and the Ludwig Center for Cancer Research of the University of Lausanne.

ACKNOWLEDGEMENTS

We gratefully acknowledge P. Gannon, M. Irving, O. Michielin, P. Romero, S. Siegert, and L. Zhang for essential collaboration and advice; N. Montandon, and M. van Overloop for outstanding technical assistance.

REFERENCES

1. Stone JD, Kranz DM. Role of T cell receptor affinity in the efficacy and specificity of adoptive T cell therapies. Front Immunol 2013;4:244.
2. Zeh HJ, 3rd, Perry-Lalley D, Dudley ME, Rosenberg SA, Yang JC. High avidity CTLs for two self-antigens demonstrate superior in vitro and in vivo antitumor efficacy. J Immunol 1999;162:989-94.
3. Holler PD, Kranz DM. Quantitative analysis of the contribution of TCR/pepMHC affinity and CD8 to T cell activation. Immunity 2003;18:255-64.
4. Tian S, Maile R, Collins EJ, Frelinger JA. CD8+ T cell activation is governed by TCR-peptide/MHC affinity, not dissociation rate. J Immunol 2007;179:2952-60.
5. Schmid DA, Irving MB, Posevitz V, Hebeisen M, Posevitz-Fejfar A, Sarria JC, et al. Evidence for a TCR affinity threshold delimiting maximal CD8 T cell function. J Immunol 2010;184:4936-46.
6. Foley MH, Forcier T, McAndrew E, Gonzalez M, Chen H, Juelg B, et al. High avidity CD8+ T cells efficiently eliminate motile hiv-infected targets and execute a locally focused program of anti-viral function. PLoS One 2014;9:e87873.
7. Tan MP, Gerry AB, Brewer JE, Melchiori L, Bridgeman JS, Bennett AD, et al. TCR binding affinity governs the functional profile of cancer-specific CD8 T cells. Clin Exp Immunol 2014.
8. Aleksic M, Liddy N, Molloy PE, Pumphrey N, Vuidepot A, Chang KM, et al. Different affinity windows for virus and cancer-specific T-cell receptors: implications for therapeutic strategies. Eur J Immunol 2012;42:3174-9.
9. Wang XL, Altman JD. Caveats in the design of MHC class I tetramer/antigen-specific T lymphocytes dissociation assays. J Immunol Methods 2003;280:25-35.

10. Schmidt J, Dojcinovic D, Guillaume P, Luescher I. Analysis, Isolation, and Activation of Antigen-Specific CD4(+) and CD8(+) T Cells by Soluble MHC-Peptide Complexes. Front Immunol 2013;4:218.

11. Nauerth M, Weissbrich B, Knall R, Franz T, Dossinger G, Bet J, et al. TCR-ligand koff rate correlates with the protective capacity of antigen-specific CD8+ T cells for adoptive transfer. Sci Transl Med 2013;5:192ra87.

12. Huang J, Zarnitsyna VI, Liu B, Edwards LJ, Jiang N, Evavold BD, et al. The kinetics of two-dimensional TCR and pMHC interactions determine T-cell responsiveness. Nature 2010;464:932-6.

13. Huppa JB, Axmann M, Mortelmaier MA, Lillemeier BF, Newell EW, Brameshuber M, et al. TCR-peptide-MHC interactions in situ show accelerated kinetics and increased affinity. Nature 2010;463:963-7.

14. Liu B, Zhong S, Malecek K, Johnson LA, Rosenberg SA, Zhu C, et al. 2D TCR-pMHC-CD8 kinetics determines T-cell responses in a self-antigen-specific TCR system. Eur J Immunol 2014;44:239-50.

15. Schmidt J, Guillaume P, Irving M, Baumgaertner P, Speiser D, Luescher IF. Reversible major histocompatibility complex I-peptide multimers containing Ni(2+)-nitrilotriacetic acid peptides and histidine tags improve analysis and sorting of CD8(+) T cells. J Biol Chem 2011;286:41723-35.

16. Derre L, Bruyninx M, Baumgaertner P, Ferber M, Schmid D, Leimgruber A, et al. Distinct sets of alphabeta TCRs confer similar recognition of tumor antigen NY-ESO-1157-165 by interacting with its central Met/Trp residues. Proc Natl Acad Sci U S A 2008;105:15010-5.

17. Purbhoo MA, Boulter JM, Price DA, Vuidepot AL, Hourigan CS, Dunbar PR, et al. The human CD8 coreceptor effects cytotoxic T cell activation and antigen sensitivity primarily by mediating complete phosphorylation of the T cell receptor zeta chain. J Biol Chem 2001;276:32786-92.

18. Zoete V, Irving M, Ferber M, Cuendet MA, Michielin O. Structure-Based, Rational Design of T Cell Receptors. Front Immunol 2013;4:268.

19. Hebeisen M, Baitsch L, Presotto D, Baumgaertner P, Romero P, Michielin O, et al. SHP-1 phosphatase activity counteracts increased T cell receptor affinity. J Clin Invest 2013;123:1044-56.

20. Irving M, Zoete V, Hebeisen M, Schmid D, Baumgartner P, Guillaume P, et al. Interplay between T cell receptor binding kinetics and the level of cognate peptide presented by major histocompatibility complexes governs CD8+ T cell responsiveness. J Biol Chem 2012;287:23068-78.

21. Holler PD, Chlewicki LK, Kranz DM. TCRs with high affinity for foreign pMHC show self-reactivity. Nat Immunol 2003;4:55-62.

22. Laugel B, van den Berg HA, Gostick E, Cole DK, Wooldridge L, Boulter J, et al. Different T cell receptor affinity thresholds and CD8 coreceptor dependence govern cytotoxic T lymphocyte activation and tetramer binding properties. J Biol Chem 2007;282:23799-810.

23. Dutoit V, Rubio-Godoy V, Doucey MA, Batard P, Lienard D, Rimoldi D, et al. Functional avidity of tumor antigen-specific CTL recognition directly correlates with the stability of MHC/peptide multimer binding to TCR. J Immunol 2002;168:1167-71.

24. La Gruta NL, Doherty PC, Turner SJ. A correlation between function and selected measures of T cell avidity in influenza virus-specific CD8+ T cell responses. Eur J Immunol 2006;36:2951-9.

25. Aleksic M, Dushek O, Zhang H, Shenderov E, Chen JL, Cerundolo V, et al. Dependence of T cell antigen recognition on T cell receptor-peptide MHC confinement time. Immunity 2010;32:163-74.

26. Dushek O, Aleksic M, Wheeler RJ, Zhang H, Cordoba SP, Peng YC, et al. Antigen potency and maximal efficacy reveal a mechanism of efficient T cell activation. Sci Signal 2011;4:ra39.

27. Govern CC, Paczosa MK, Chakraborty AK, Huseby ES. Fast on-rates allow short dwell time ligands to activate T cells. Proc Natl Acad Sci U S A 2010;107:8724-9.

28. Luescher IF, Vivier E, Layer A, Mahiou J, Godeau F, Malissen B, et al. CD8 modulation of T-cell antigen receptor-ligand interactions on living cytotoxic T lymphocytes. Nature 1995;373:353-6.

29. Gao GF, Tormo J, Gerth UC, Wyer JR, McMichael AJ, Stuart DI, et al. Crystal structure of the complex between human CD8alpha(alpha) and HLA-A2. Nature 1997;387:630-4.

30. Wooldridge L, van den Berg HA, Glick M, Gostick E, Laugel B, Hutchinson SL, et al. Interaction between the CD8 coreceptor and major histocompatibility complex class I stabilizes T cell receptor-antigen complexes at the cell surface. J Biol Chem 2005;280:27491-501.

31. Puech PH, Nevoltris D, Robert P, Limozin L, Boyer C, Bongrand P. Force measurements of TCR/pMHC recognition at T cell surface. PLoS One 2011;6:e22344.

32. Artyomov MN, Lis M, Devadas S, Davis MM, Chakraborty AK. CD4 and CD8 binding to MHC molecules primarily acts to enhance Lck delivery. Proc Natl Acad Sci U S A 2010;107:16916-21.

33. Jiang N, Huang J, Edwards LJ, Liu B, Zhang Y, Beal CD, et al. Two-stage cooperative T cell receptor-peptide major histocompatibility complex-CD8 trimolecular interactions amplify antigen discrimination. Immunity 2011;34:13-23.

34. Cole DK, Laugel B, Clement M, Price DA, Wooldridge L, Sewell AK. The molecular determinants of CD8 co-receptor function. Immunology 2012;137:139-48.

35. Zhu Z, Singh V, Watkins SK, Bronte V, Shoe JL, Feigenbaum L, et al. High-avidity T cells are preferentially tolerized in the tumor microenvironment. Cancer Res 2013;73:595-604.

36. Johnson LA, Morgan RA, Dudley ME, Cassard L, Yang JC, Hughes MS, et al. Gene therapy with human and mouse T-cell receptors mediates cancer regression and targets normal tissues expressing cognate antigen. Blood 2009;114:535-46.

37. Morgan RA, Chinnasamy N, Abate-Daga D, Gros A, Robbins PF, Zheng Z, et al. Cancer regression and neurological toxicity following anti-MAGE-A3 TCR gene therapy. J Immunother 2013;36:133-51.

Table 1. Kinetic characteristics of HLA-A*0201/NY-ESO-$1_{157-165}$-specific TCR variants

	SPR TCR-pMHC kinetics (b)				NTAmer dissociation kinetics				NTAmer$^{227-228}$ dissociation kinetics			
	Soluble TCRs				CD8+ (c)		CD8- (c)		CD8+ (c)		CD8- (c)	
TCR variants (a)	K_D μM	k_{on} $M^{-1}s^{-1}$ $x10^4$	k_{off} s^{-1} $x10^{-2}$	$t_{1/2}$ s	k_{off} s^{-1} $x10^{-2}$	$t_{1/2}$ s	k_{off} s^{-1} $x10^{-2}$	$t_{1/2}$ s	k_{off} s^{-1} $x10^{-2}$	$t_{1/2}$ s	k_{off} s^{-1} $x10^{-2}$	$t_{1/2}$ s
V49I	n.a	n.a	n.a	n.a	21.21	3	n.a	n.a	n.a	n.a	n.a	n.a
Wild-type	21.4	1.1	23.0	3	4.08	17	10.2	7	11.2	6	15.4	5
G50A	4.62	1.5	6.9	10	1.47	47	n.d	n.d	5.28	13	n.d	n.d
A97L	2.69	2.3	6.1	11	1.60	44	n.d	n.d	4.70	15	n.d	n.d
DMβ	1.91	2.4	4.5	15	0.78	90	2.76	25	3.02	23	3.15	22
TMβ	0.91	1.4	1.3	53	0.28	247	1.03	67	0.87	79	0.97	72
TMα	0.40	12.1	4.8	14	0.44	158	n.d	n.d	1.76	40	n.d	n.d
QMα	0.14	10.9	1.5	46	0.21	341	0.80	87	0.74	94	0.75	92
Wtc51m	0.015	8.5	0.13	533	0.05	1505	0.14	497	0.15	475	0.14	496

(a) Wild-type TCR (BC1; AV23.1/BV13.1) was isolated from melanoma patient LAU 155 (16) and a panel of TCR variants of progressive increasing affinities against HLA-A*0201/NY-ESO-$1_{157-165}$ was established as described in (20).

(b) TCR-pMHC affinity, k_{off} and k_{on} values were previously measured by SPR as reported in (20).

(c) CD8+ T cells, TCR-transduced SUP-T1 cells; CD8- T cells, TCR-transduced Jurkat cells.

n.a, not applicable; n.d, not done.

FIGURE LEGENDS

Figure 1. Assessment of monomeric dissociation kinetics by reversible NTAmers. (A) Basic illustration of the off-rate (k_{off}) dissociation assay. Human CD8+ antigen-specific T cells were first stained with HLA-A*0201/tumor antigen-specific NTAmers containing PE-labeled backbone (green) and Cy5-labeled monomers (red) carrying imidazole-sensitive Ni^{2+}-NTA_4 moieties. Upon addition of imidazole, the NTAmer multimeric complex rapidly dissociated into Cy5-labeled pMHC monomers releasing the SA-PE NTA_4 molecules. Decay of Cy5 fluorescence was visualized by high-resolution microscopy flow cytometry **(B)** or conventional flow cytometry over time **(C)** using SUP-T1 cells engineered with TCRs of incremental affinity for the tumor antigen A2/ NY-ESO-$1_{157-165}$ (20) (Table 1). **(B)** Differential interference contrast (DIC), PE, Cy5 and PE/Cy5 composite images are shown at the indicated time-points. **(C)** Representative dot plots from FACS-based dissociation curves (Cy5-labeled pMHC monomers) from TCR-transduced SUP-T1 cells. Decay of PE-labeled NTA_4 scaffold moieties is depicted alongside. **(D)** Temperature-controlled (15^{o}C) TCR-pMHC monomeric dissociation off-rates (Cy5-monomers, blue circles) were assessed upon addition of imidazole (t = 0) within the entire panel of TCR-transduced SUP-T1 cells. Data best fitted a one-phase exponential decay equation after subtraction of non-specific background and are expressed as % of maximal binding, normalized to 100% and plotted over time. Decay of SA-PE-NTA_4 fluorescence (white circles) from NTAmers occurred within the first 2-3 seconds upon imidazole addition and was independent TCR-pMHC affinity. Time for half maximal binding ($t_{1/2}$) was determined and average half-life value ($t_{1/2}$) of > 3 independent experiments is depicted in second (s) for each TCR engineered SUP-T1 cell variant. Untransduced SUP-T1 cells; no TCR. N/A; not applicable.

Figure 2. Contribution of CD8 binding to TCR-pMHC dissociation kinetics. (A) Positive correlations (Pearson coefficient r and p value) obtained between surface-based monomeric half-lives ($t_{1/2}$) with wild-type NTAmers (monomer, blue line) or CD8-binding deficient NTAmers$^{227-228}$ (monomer$^{227-228}$, red line) on CD8+ TCR-transduced SUP-T1 cells, and monomeric half-lives ($t_{1/2}$) and affinities (equilibrium dissociation constant K_D) as measured by SPR on soluble TCRs. Weaker correlations were found when assessing half-lives using a pure grade tetramer assay (opened circles). **(B)** Direct comparison of wild-type (blue circles) and CD8-binding deficient (red diamonds) monomeric dissociation half-lives by NTAmers (> 3 independent experiments). The impact of CD8 binding is shown as fold change (grey histograms) for each TCR-transduced SUP-T1 variant. **(C)** Representative first order monomeric TCR-pMHC dissociation curves detected upon addition of imidazole at 15^{o}C (t = 0) for CD8-null Jurkat T cells engineered with the indicated TCR variants (expressed as % of maximal binding over time) and labeled with wild-type NTAmers (monomer, blue circles) or CD8-binding deficient NTAmers$^{227-228}$ (monomer$^{227-228}$, red circles). Decay of PE-NTA_4 fluorescence (white circles) is also represented. Average dissociation half-life value (of 3 independent experiments) with wild-type NTAmers or NTAmers$^{227-228}$ is shown for each TCR-transduced Jurkat T cell variant. **(D)** Positive correlations (Pearson coefficient r and p values) between surface-based monomeric half-lives ($t_{1/2}$) with wild-type NTAmer (monomer, blue line) or CD8-binding deficient NTAmer$^{227-228}$ (monomer$^{227-228}$, red line) on TCR-transduced CD8-null Jurkat T cells, and monomeric half-lives ($t_{1/2}$) by SPR on soluble TCR variants.

Figure 3. Relationship between cell-surface monomeric dissociation kinetics and calcium flux. (A-C) Intracellular calcium mobilization of CD8+ SUP-T1 cells expressing TCRs of

incremental affinities for pMHC before (baseline) and over time after stimulation with 1μg/ml A2/NY-ESO-$1_{157-165}$-specific multimers (blue circles) or 1 μg/ml CD8-binding deficient A2/NY-ESO-$1_{157-165}$-specific multimers$^{227-228}$ (red diamonds). A representative kinetic analysis of calcium mobilization is depicted in **(A)** and the mean calcium flux values of 4 independent experiments are plotted as Ca^{2+} peak MFI ($x10^4$) in **(B)** together with maximal calcium flux induced after ionomycin stimulation. **(C)** Correlation (Pearson coefficient r and p value) between calcium flux peak MFI and dissociation k_{off} rates for SUP-T1 cells expressing TCRs within the physiological affinity range (blue circles). Calcium flux values for SUP-T1 cells expressing supraphysiological affinity TCRs (TMα, QMα and wtc51m) (blue stars), and those obtained after stimulation with CD8-binding deficient multimers$^{227-228}$ (red diamonds) are shown, but were not included in the correlative analysis. **(D)** A representative kinetic analysis of calcium mobilization in primary TCR-transduced CD8+ T cells before (no antigen-presenting cells; APC) and after stimulation with T2 cells pulsed with graded concentration of the analog NY-ESO-$1_{157-165}$ peptide (SLLMWITQA) or ionomycin as positive control. **(E)** The mean calcium flux values were plotted as Ca^{2+} peak MFI with varying peptide concentration for each primary CD8+ TCR-transduced T cell variant. No calcium flux was detected upon stimulation of wild-type (WT) NY-ESO-1-transduced T cells with Flu-specific peptide (Flu) or no APCs. **(F)** Correlation (Pearson coefficient r and p value) between half-maximal calcium mobilization capacity (Ca^{2+} EC_{50}) and NTAmer-based dissociation k_{off} values for T cells expressing TCRs within the physiological affinity range (gray circles). Calcium flux values obtained for CD8+ T cells expressing TCRs of supraphysiological affinities (TMα, QMα and wtc51m) are shown (blue stars), but were not included in the correlative analysis.

Figure 4. Relationship between cell-surface monomeric dissociation kinetics and target cell killing. Experiments were performed on A2/NY-ESO-$1_{157-165}$-specific CD8+ T cell clones (n = 20) expressing eight well-defined TCRαβ clonotypes, derived from melanoma patient LAU 155 as previously described (16). **(A)** Representative first-order monomeric dissociation curves obtained upon addition of imidazole at 4^oC (t = 0) for tumor-specific T cell clones stained with A2/NY-ESO-$1_{157-165}$-specific-NTAmers. Average half-lives ($t_{1/2}$) determined from each distinct TCRαβ clonotypes (n = 2 to 3 independent sister T cell clones) are indicated and were highly reproducible in two independent experiments (data not shown). **(B)** The relative functional avidity of tumor-specific T cell clones expressing distinct TCRαβ clonotypes was assessed by measuring their lytic capacity for T2 target cells ($A2^{pos}$; $TAP^{neg/neg}$) pulsed with graded concentration of the natural NY-ESO-$1_{157-165}$ peptide (SLLMWITQC). **(C)** Correlations (Pearson coefficient r and p value) between relative functional avidity (EC_{50}, peptide concentration used to achieve 50% of maximal lysis) and monomeric TCR-pMHC dissociation k_{off} values. Mean EC_{50} values of 3 independent experiments. **(D)** Tumor reactivity by tumor-specific T cell clonotypes for the melanoma cell line Me275 ($A2^{pos}$/NY-ESO-$1_{157-165}{}^{pos}$) at the indicated effector:target (E:T) ratio. **(E)** Correlations (Pearson coefficient r and p value) between melanoma cell killing (mean % of specific lysis at the E:T ratio of 10:1 from 2 independent experiments) and monomeric TCR-pMHC dissociation k_{off} values.

Figure 5. High-throughput screen of functionally relevant tumor-specific CD8+ T cells by NTAmers. Relationship between functional avidity and monomeric TCR-pMHC k_{off} rates of a large panel of tumor-specific CD8+ T cell clones specific for A2/NY-ESO-$1_{157-165}$ **(A-C)** or A2/Melan-$A^{MART-1}{}_{26-35}$ **(D-F)** tumor antigen and derived from melanoma patient LAU 50 and

LAU 618 respectively. **(A, D)** Representative first order dissociation curves obtained after addition of imidazole at 4°C for CD8+ A2/NY-ESO-$1_{157-165}$-specific T cell clones (LAU 50; n = 67) and A2/Melan-A^{MART-1}_{26-35}-specific T cell clones (LAU 618, n = 80) respectively, stained with specific NTAmers and arbitrarily separated into short (white circles) or long (black squares) half-lives according to their $t_{1/2}$ values. **(B, E)** Relative functional avidity on a selection of A2/NY-ESO-$1_{157-165}$-specific T cell clones (n = 23) or A2/ Melan-A^{MART-1}_{26-35}-specific T cell clones (n = 34) of short or long half-lives using T2 target cells pulsed with graded concentration of natural NY-ESO-$1_{157-165}$- or Melan-A^{MART-1}_{26-35}-specific peptide. **(C, F)** Positive correlations (Spearman coefficient r and p value) obtained between relative functional avidity by EC_{50} (50% of maximal target cell killing) and monomeric TCR-pMHC dissociation k_{off} values. Each data-point represents the result of an individual tumor-specific T cell clone, averaged from 2 independent experiments.

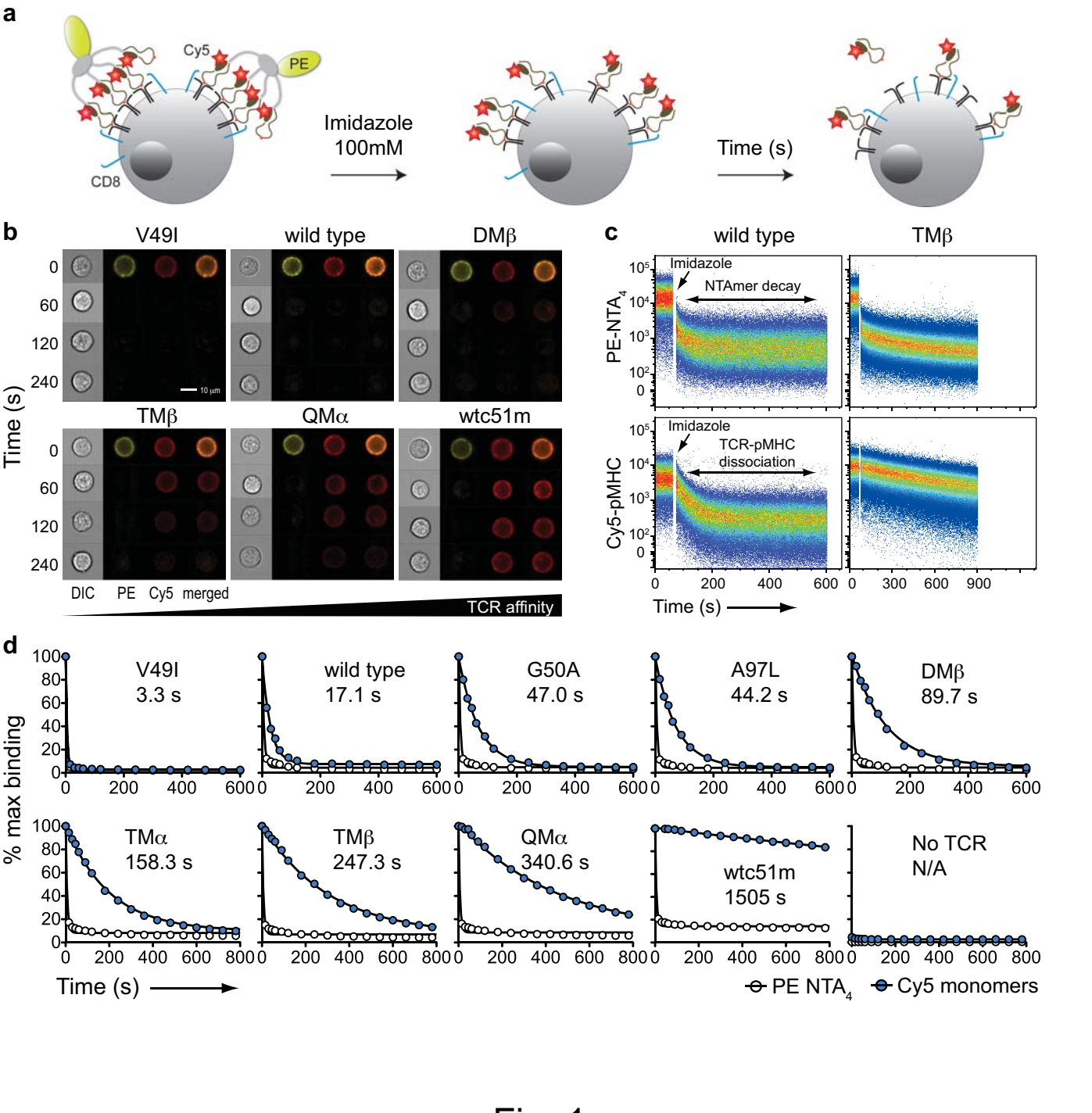
a
Cy5
PE
CD8
Imidazole
100mM
Time (s)
b
V49I
wild type
DMβ
TMβ
QMα
wtc51m
Time (s)
0
60
120
240
10 μm
DIC
PE
Cy5
merged
TCR affinity
c
wild type
TMβ
Imidazole
NTAmer decay
PE-NTA4
Imidazole
TCR-pMHC
dissociation
Cy5-pMHC
Time (s)
d
% max binding
V49I
3.3 s
wild type
17.1 s
G50A
47.0 s
A97L
44.2 s
DMβ
89.7 s
TMα
158.3 s
TMβ
247.3 s
QMα
340.6 s
wtc51m
1505 s
No TCR
N/A
Time (s)
PE NTA4
Cy5 monomers

-- Fig. 1 --

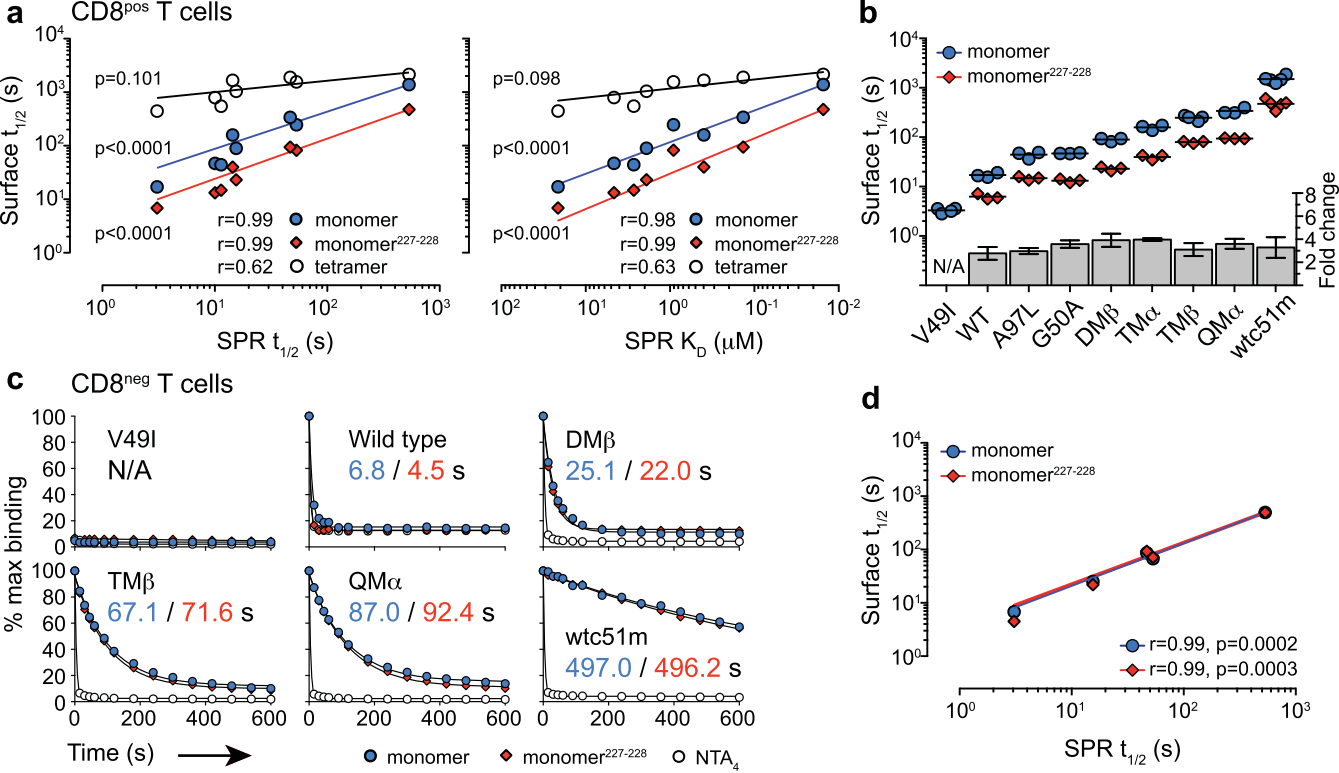
a
CD8pos T cells
Surface t1/2 (s)
p=0.101
p<0.0001
p<0.0001
r=0.99 monomer
r=0.99 monomer227-228
r=0.62 tetramer
SPR t1/2 (s)
p=0.098
p<0.0001
p<0.0001
r=0.98 monomer
r=0.99 monomer227-228
r=0.63 tetramer
SPR KD (μM)
b
monomer
monomer227-228
Surface t1/2 (s)
N/A
Fold change
V49I
WT
A97L
G50A
DMβ
TMα
TMβ
QMα
wtc51m
c
CD8neg T cells
% max binding
V49I
N/A
Wild type
6.8 / 4.5 s
DMβ
25.1 / 22.0 s
TMβ
67.1 / 71.6 s
QMα
87.0 / 92.4 s
wtc51m
497.0 / 496.2 s
Time (s)
monomer
monomer227-228
NTA4
d
monomer
monomer227-228
Surface t1/2 (s)
r=0.99, p=0.0002
r=0.99, p=0.0003
SPR t1/2 (s)

-- Fig. 2 --

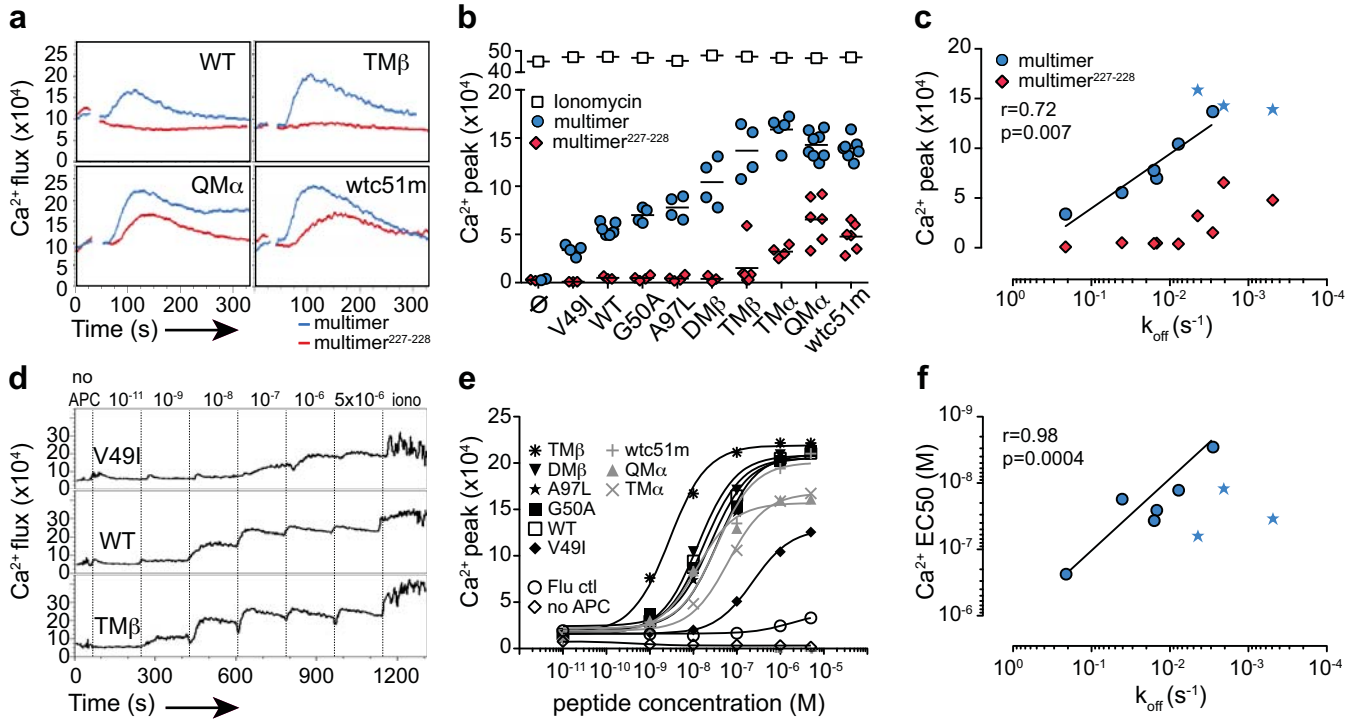
a
WT
TMβ
QMα
wtc51m
Ca2+ flux (x10⁴)
Time (s)
multimer
multimer227-228
b
Ionomycin
multimer
multimer227-228
Ca2+ peak (x10⁴)
Ø
V49I
WT
G50A
A97L
DMβ
TMβ
TMα
QMα
wtc51m
c
multimer
multimer227-228
r=0.72
p=0.007
Ca2+ peak (x10⁴)
koff (s-1)
d
no APC
10-11
10-9
10-8
10-7
10-6
5x10-6
iono
V49I
WT
TMβ
Ca2+ flux (x10⁴)
Time (s)
e
TMβ
DMβ
A97L
G50A
WT
V49I
wtc51m
QMα
TMα
Flu ctl
no APC
Ca2+ peak (x10⁴)
peptide concentration (M)
f
r=0.98
p=0.0004
Ca2+ EC50 (M)
koff (s-1)

-- Fig. 3 --

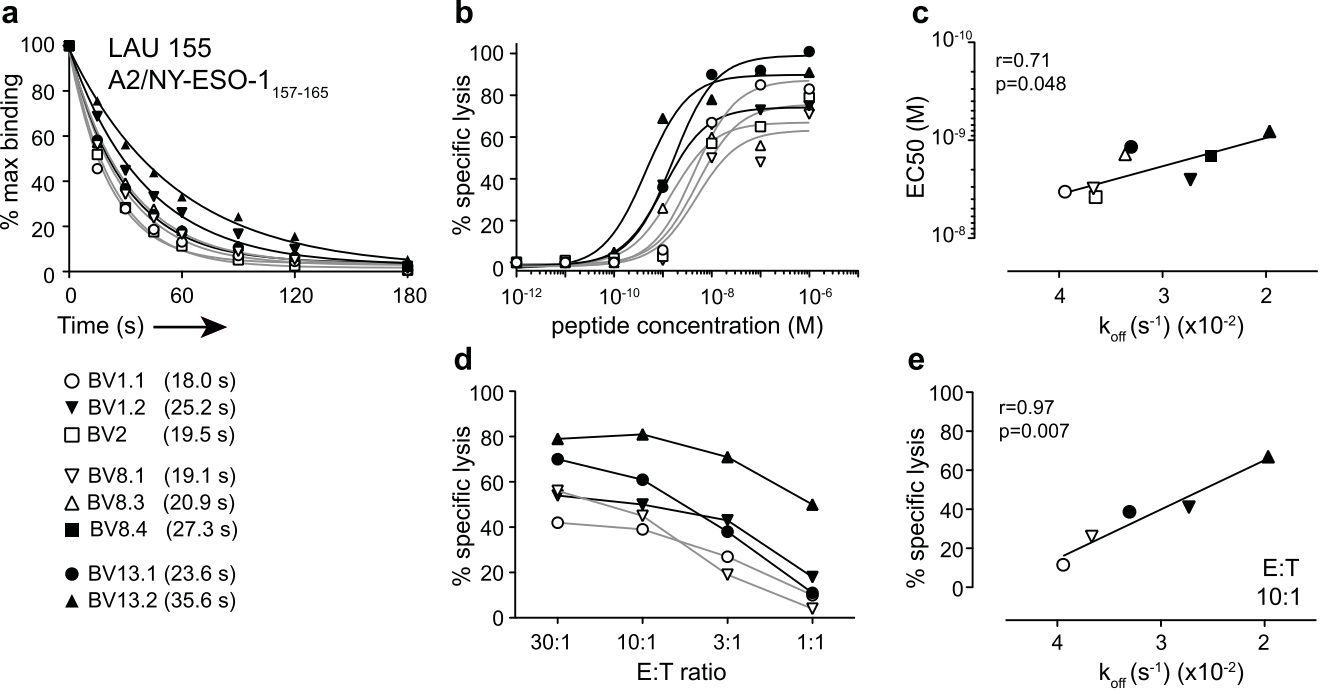
a
LAU 155
A2/NY-ESO-1 157-165
% max binding
Time (s)
BV1.1 (18.0 s)
BV1.2 (25.2 s)
BV2 (19.5 s)
BV8.1 (19.1 s)
BV8.3 (20.9 s)
BV8.4 (27.3 s)
BV13.1 (23.6 s)
BV13.2 (35.6 s)
b
% specific lysis
peptide concentration (M)
c
r=0.71
p=0.048
EC50 (M)
koff (s-1) (x10-2)
d
% specific lysis
E:T ratio
e
r=0.97
p=0.007
% specific lysis
E:T 10:1
koff (s-1) (x10-2)

-- Fig. 4 --

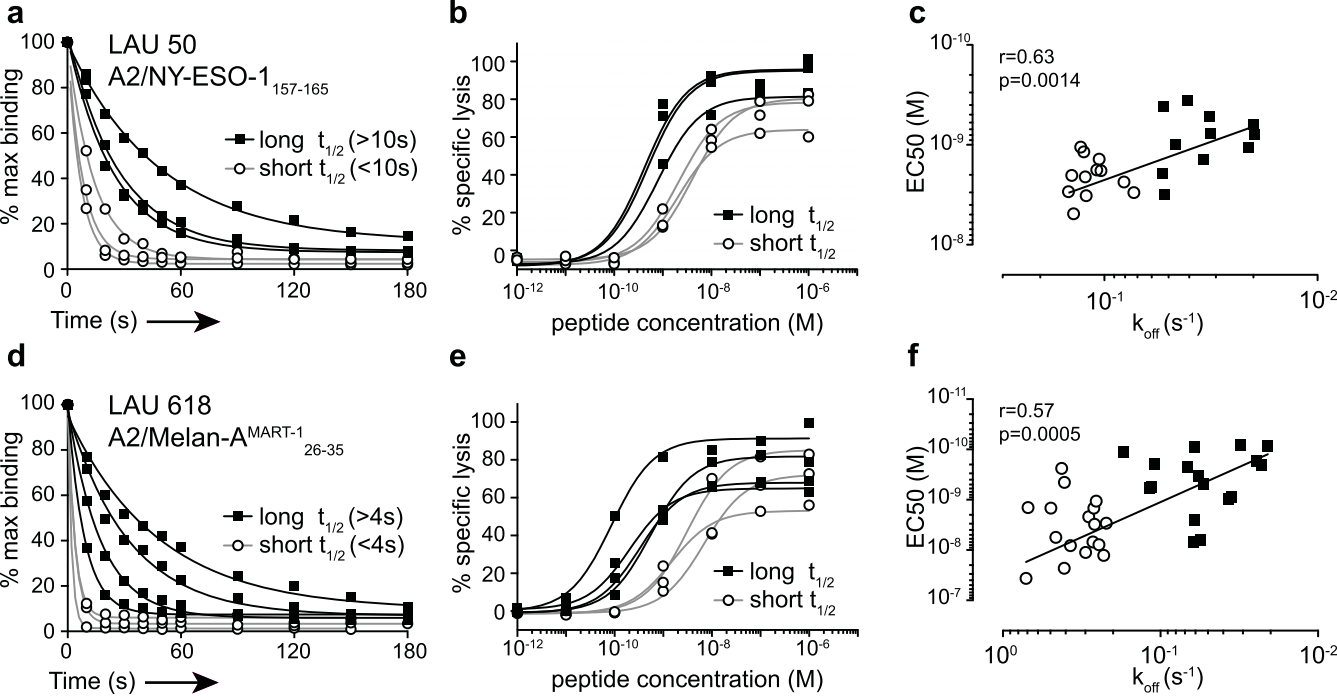
a
LAU 50
A2/NY-ESO-1 157-165
long t1/2 (>10s)
short t1/2 (<10s)
% max binding
Time (s)
b
% specific lysis
peptide concentration (M)
c
r=0.63
p=0.0014
EC50 (M)
koff (s-1)
d
LAU 618
A2/Melan-A MART-1 26-35
long t1/2 (>4s)
short t1/2 (<4s)
% max binding
Time (s)
e
% specific lysis
peptide concentration (M)
f
r=0.57
p=0.0005
EC50 (M)
koff (s-1)

-- Fig. 5 --

SUPPLEMENTARY FIGURE LEGENDS

Supplementary Figure S1. Determination of TCR-ligand off-rates on a panel of CD8+ T cells engineered with TCRs of incremental affinities against the A2/NY-ESO-1 tumor antigen. (A and B) FACS-based TCR-pMHC dissociation curves for each TCR-transduced SUP-T1 cell variant are depicted after staining with wild-type HLA-A*0201/NY-ESO-$1_{157-165}$ -specific NTAmers **(A)** or CD8 binding-deficient HLA-A*0201/ NY-ESO-$1_{157-165}$ -specific NTAmers$^{227-228}$ **(B)**. Imidazole (100 mM) was added after 1 minute of baseline recording and monomeric pMHC dissociation was followed in the Cy5 channel during 10 to 15 minutes at constant temperature (15^{o}C). **(C)** Monomeric TCR-pMHC dissociation rates, following reversible wild-type NTAmer (monomer, blue circles) or CD8-binding-deficient NTAmer$^{227-228}$ (monomer$^{227-228}$, red diamonds) staining, were analyzed in Prism and best fitted a first order monomeric decay function after subtraction of non-specific background. Average half-life values (in second, s) of > 3 independent experiments are depicted for each TCR-transduced SUP-T1 cell variant and were highly reproducible between two different investigators (data not shown). Of note, no NTAmer staining was detected in untransduced SUP-T1 cells (no TCR). N/A; not applicable.

Supplementary Figure S2. Relationship between monomeric off-rates by reversible NTAmers and monomeric off-rates and affinity by SPR. (A) Correlations (Pearson coefficient r and p value) between surface-based TCR-pMHC off-rates (k_{off}) with A2/NY-ESO-$1_{157-165}$ -specific NTAmers (monomer, blue circles), CD8-binding deficient NTAmers$^{227-228}$ (monomer$^{227-228}$, red diamonds) or pure grade tetramers (white circles) on CD8+ TCR-transduced SUP-T1 cells, and monomeric off-rates (k_{off}) (left panel) and affinities (equilibrium dissociation constant K_D) (right panel) values as measured by SPR on soluble TCR variants. **(B)** Correlations (Pearson coefficient r and p value) between surface-based TCR-pMHC off-rates (k_{off}) with A2/NY-ESO-$1_{157-165}$ -specific NTAmers (monomer, blue circles) or CD8-binding deficient NTAmers$^{227-228}$ (monomer$^{227-228}$, red diamonds) on CD8- TCR-transduced Jurkat T cells, and monomeric off-rates (k_{off}) and affinities (K_D) values as measured by SPR on soluble TCR variants. Of note, similar correlations were obtained between NTAmers and NTAmers$^{227-228}$ on TCR-transduced Jurkat T cells lacking CD8

expression **(B)** and were highly similar to those found by NTAmers$^{227\text{-}228}$ on CD8+ SUP-T1 cells **(A)**.

Supplementary Figure S3. Monomeric dissociation half-lives of naturally occurring or vaccine-induced tumor-specific CD8+ T cell clones from three melanoma patients. (A) Representative examples of NTAmer-based dissociation kinetics of A2/NY-ESO-$1_{157\text{-}165}$-specific CD8+ T cell clones expressing well-defined TCRαβ clonotypes isolated from melanoma patient LAU 155 as described in (1). **(B)** Representative examples of NTAmer-based dissociation kinetics of a large panel of A2/NY-ESO-$1_{157\text{-}165}$ CD8+ T cell clones from melanoma patient LAU 50 with naturally occurring anti-tumor CD8+ T cell responses. **(C)** Representative examples of NTAmer-based dissociation kinetics of A2/Melan-$A^{MART\text{-}1}{}_{26\text{-}35}$-specific CD8+ T cell clones from melanoma patient LAU 618 following Melan-$A^{MART\text{-}1}{}_{26\text{-}35}$ peptide vaccination and CpG oligodeoxynucleotide 7909 as adjuvant. Imidazole was added after 1 minute **(A)** or 30 seconds **(B and C)** of baseline recording and monomeric dissociation was followed in the Cy5 channel at constant temperature (4^oC) during 3 to 5 minutes. **(A-C)** Data are expressed as % of maximal binding after subtraction of non-specific background, normalized to 100% and plotted over time (in seconds). Monomeric TCR-pMHC dissociation rates were analyzed in Prism and best fitted a first order monomeric decay function.

Supplementary Figure S4. Monomeric TCR-pMHC kinetics of tumor-specific CD8+ T cell subpopulations according to the TRBV repertoire usage. NTAmer-based dissociation half-lives were assessed on A2/NY-ESO-$1_{157\text{-}165}$-specific CD8+ T cell clones derived from melanoma patient LAU 50 (n = 50) **(A)** and A2/Melan-$A^{MART\text{-}1}{}_{26\text{-}35}$-specific CD8+ T cell clones (n = 70) from melanoma patient LAU 618 **(B)** and distributed according to the expression of TCR Vβ family usage by using anti-BV monoclonal antibodies (mAb) and flow cytometry. Of note, a convenient feature of the anti-BV13 and anti-BV17 mAb reactivity allowed us to clearly discriminate between bright/high and dim tumor-specific T cells.

Supplementary Figure S5. Impact of rapid association on-rates on cell surface dissociation kinetics by reversible NTAmers. Comparison of first order monomeric TCR-pMHC dissociation kinetics obtained with NY-ESO-$1_{157-165}$-specific NTAmers (monomer, blue symbols) or CD8-binding deficient NTAmers$^{227-228}$ (monomer$^{227-228}$, red symbols) between two pairs of TCR variants among the panel of CD8+ SUP-T1 cells, DMβ/TMα (top) and TMβ/QMα (bottom). These pairs express TCRs differing solely for αS53W, a TCR-alpha chain mutation known to significantly increase the association k_{on} rates (TMα, $12.1x10^4$ and QMα, $10.9x10^4$ $M^{-1}s^{-1}$) while sharing similar dissociation k_{off} rates by SPR(2) (see **Table 1**). The impact of αS53W mutation between each TCR pair on the dissociation half-lives by NTAmers and NTAmers$^{227-228}$ is indicated as average fold difference from 3 independent experiments. Of note, rapid k_{on} rates have been proposed to allow rapid rebinding of the TCR to the same pMHC without complete dissociation, thus prolonging effective dissociation half-lives when k_{on} surpasses a threshold rate of 4.5 to $6x10^4$ $M^{-1}s^{-1}$ as measured by SPR(3). This phenomenon of rapid rebinding is referred as the "confinement time" of a TCR-pMHC interaction and clarifies the role of k_{on} in T cell activation(4). The differential experimental settings between NTAmer-based (cell surface of living cells) and molecular SPR-based measurements (plate bound with microflow system) may explain our observation that TCR variants with faster k_{on} showed prolonged dissociation half-lives by NTAmers. Similar data were found when using CD8-binding deficient NTAmers$^{227-228}$, suggesting that enhanced effective dissociation half-life is independent of the CD8-pMHC binding interaction.

References

1. Derre L, Bruyninx M, Baumgaertner P, Ferber M, Schmid D, Leimgruber A, et al. Distinct sets of alphabeta TCRs confer similar recognition of tumor antigen NY-ESO-1157-165 by interacting with its central Met/Trp residues. Proc Natl Acad Sci U S A 2008;105:15010-5.
2. Irving M, Zoete V, Hebeisen M, Schmid D, Baumgartner P, Guillaume P, et al. Interplay between T cell receptor binding kinetics and the level of cognate peptide presented by major histocompatibility complexes governs CD8+ T cell responsiveness. J Biol Chem 2012;287:23068-78.

3. Govern CC, Paczosa MK, Chakraborty AK, Huseby ES. Fast on-rates allow short dwell time ligands to activate T cells. Proc Natl Acad Sci U S A 2010;107:8724-9.
4. Aleksic M, Dushek O, Zhang H, Shenderov E, Chen JL, Cerundolo V, et al. Dependence of T cell antigen recognition on T cell receptor-peptide MHC confinement time. Immunity 2010;32:163-74.

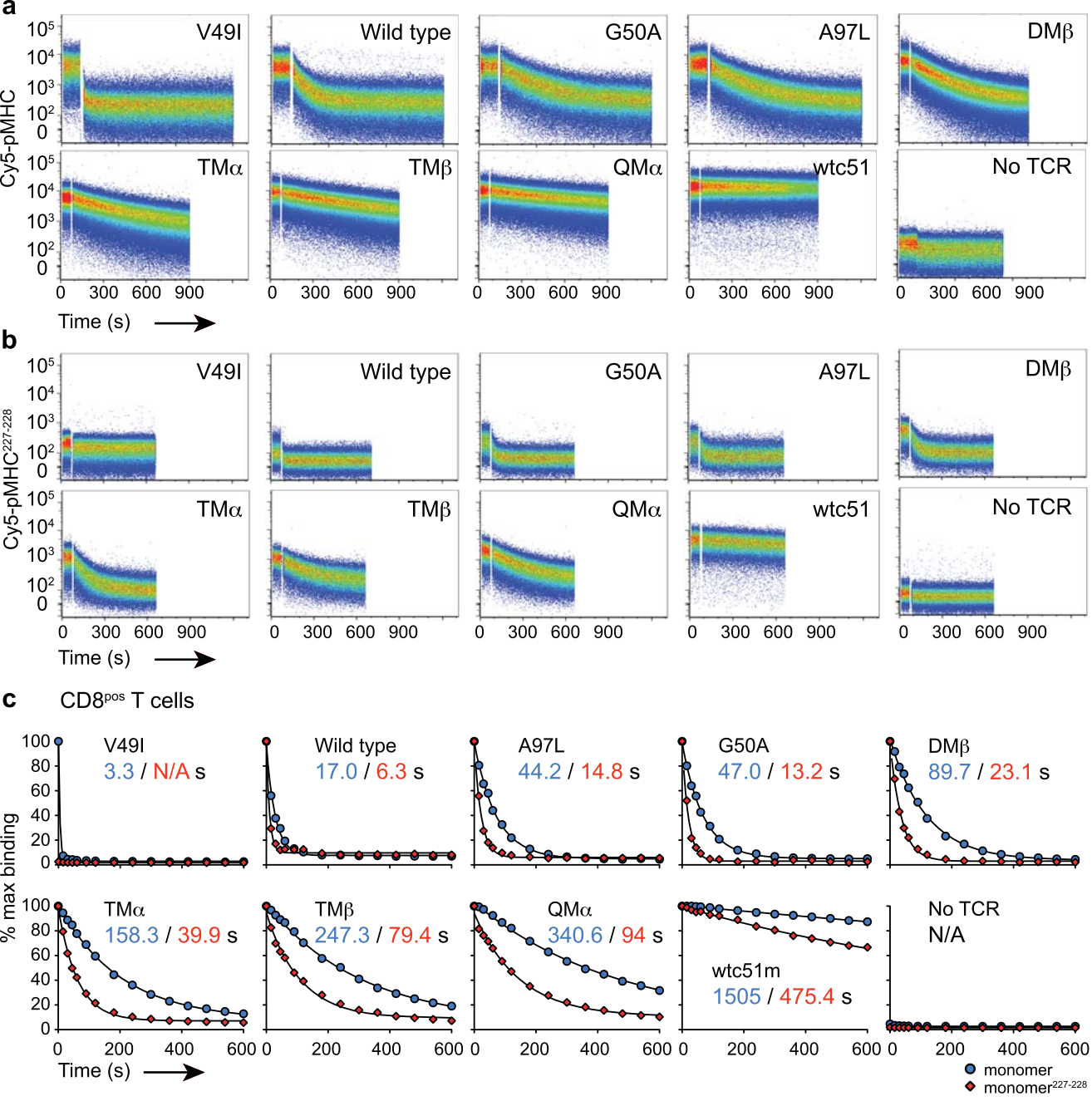
a
Cy5-pMHC
V49I
Wild type
G50A
A97L
DMβ
TMα
TMβ
QMα
wtc51
No TCR
Time (s)
b
Cy5-pMHC227-228
c
CD8pos T cells
% max binding
V49I
3.3 / N/A s
Wild type
17.0 / 6.3 s
A97L
44.2 / 14.8 s
G50A
47.0 / 13.2 s
DMβ
89.7 / 23.1 s
TMα
158.3 / 39.9 s
TMβ
247.3 / 79.4 s
QMα
340.6 / 94 s
wtc51m
1505 / 475.4 s
No TCR
N/A
monomer
monomer227-228

-- SUP. FIG.1 --

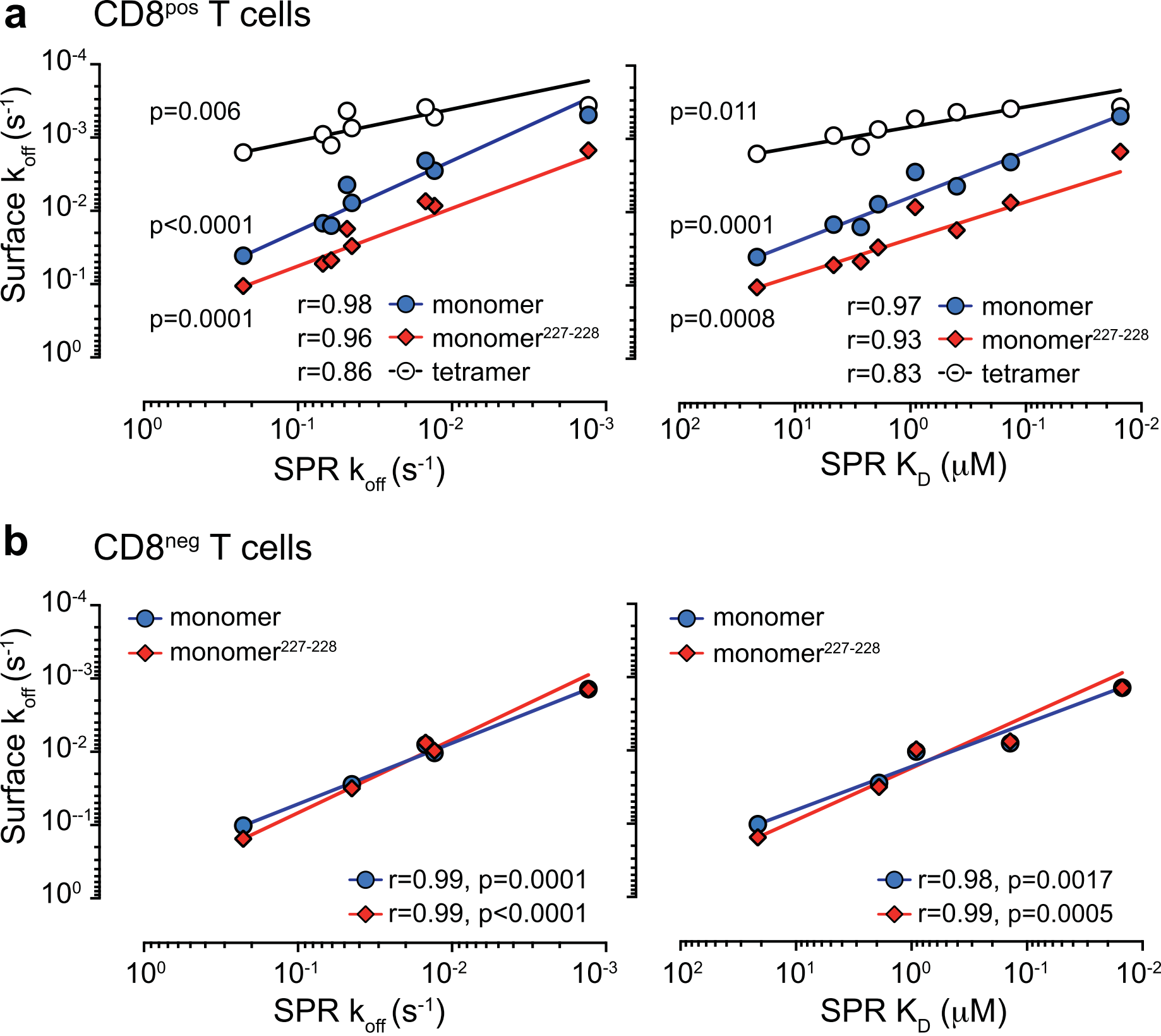
a
CD8pos T cells
Surface koff (s-1)
p=0.006
p<0.0001
p=0.0001
r=0.98 monomer
r=0.96 monomer227-228
r=0.86 tetramer
SPR koff (s-1)
p=0.011
p=0.0001
p=0.0008
r=0.97 monomer
r=0.93 monomer227-228
r=0.83 tetramer
SPR KD (μM)
b
CD8neg T cells
monomer
monomer227-228
r=0.99, p=0.0001
r=0.99, p<0.0001
r=0.98, p=0.0017
r=0.99, p=0.0005

-- Sup. Fig.2 --

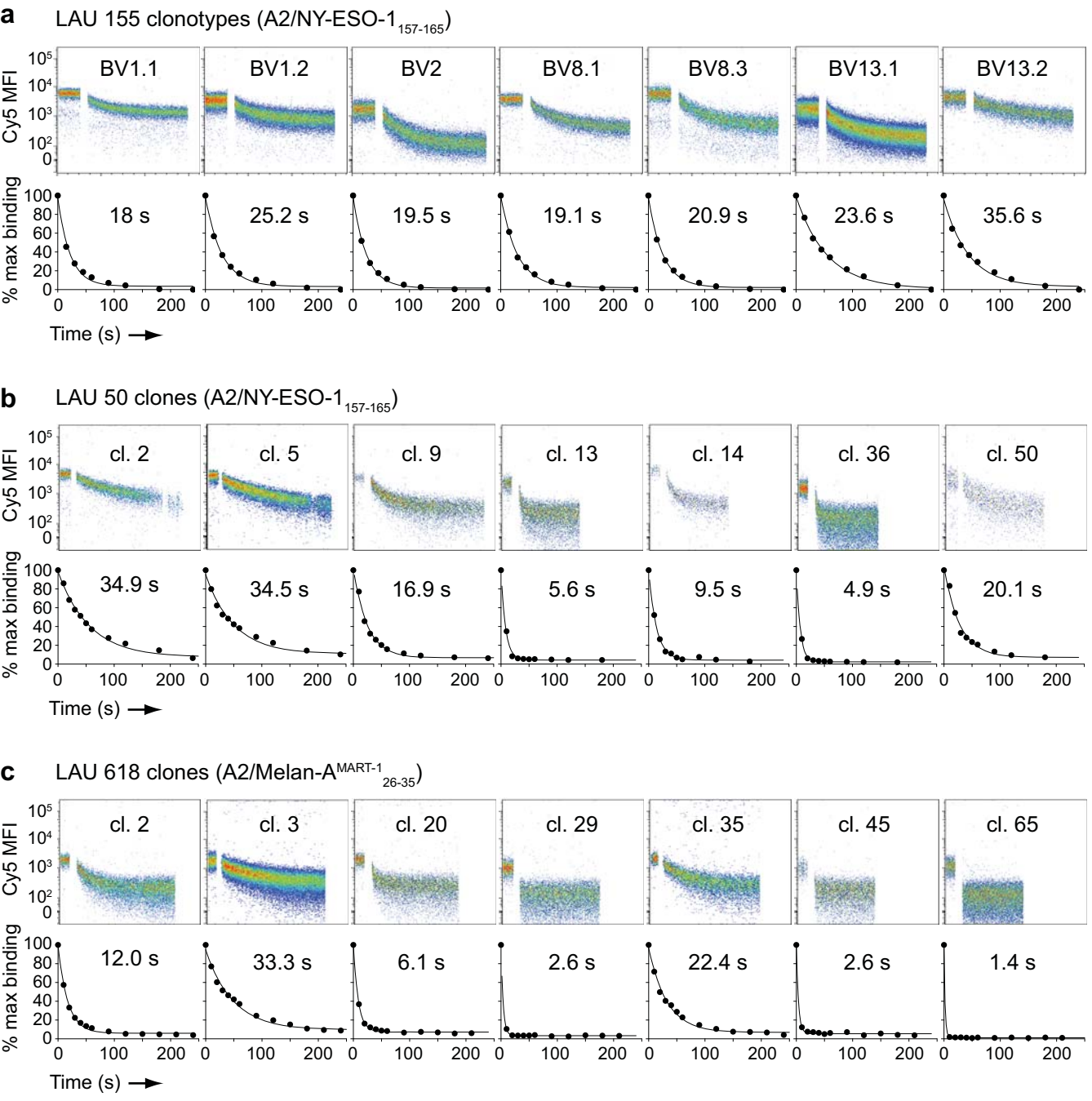
a
LAU 155 clonotypes (A2/NY-ESO-1157-165)
Cy5 MFI
BV1.1
BV1.2
BV2
BV8.1
BV8.3
BV13.1
BV13.2
% max binding
18 s
25.2 s
19.5 s
19.1 s
20.9 s
23.6 s
35.6 s
Time (s)
b
LAU 50 clones (A2/NY-ESO-1157-165)
cl. 2
cl. 5
cl. 9
cl. 13
cl. 14
cl. 36
cl. 50
34.9 s
34.5 s
16.9 s
5.6 s
9.5 s
4.9 s
20.1 s
c
LAU 618 clones (A2/Melan-AMART-126-35)
cl. 2
cl. 3
cl. 20
cl. 29
cl. 35
cl. 45
cl. 65
12.0 s
33.3 s
6.1 s
2.6 s
22.4 s
2.6 s
1.4 s

-- Sup. Fig. 3 --

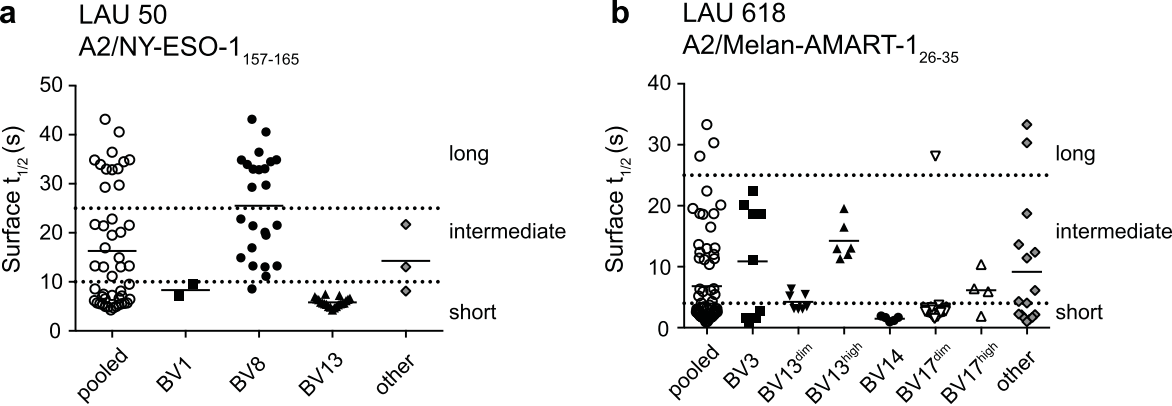
a
LAU 50
A2/NY-ESO-1 157-165
Surface t1/2 (s)
50
40
30
20
10
0
long
intermediate
short
pooled
BV1
BV8
BV13
other
b
LAU 618
A2/Melan-AMART-1 26-35
Surface t1/2 (s)
40
30
20
10
0
long
intermediate
short
pooled
BV3
BV13dim
BV13high
BV14
BV17dim
BV17high
other

-- Sup. Fig.4 --

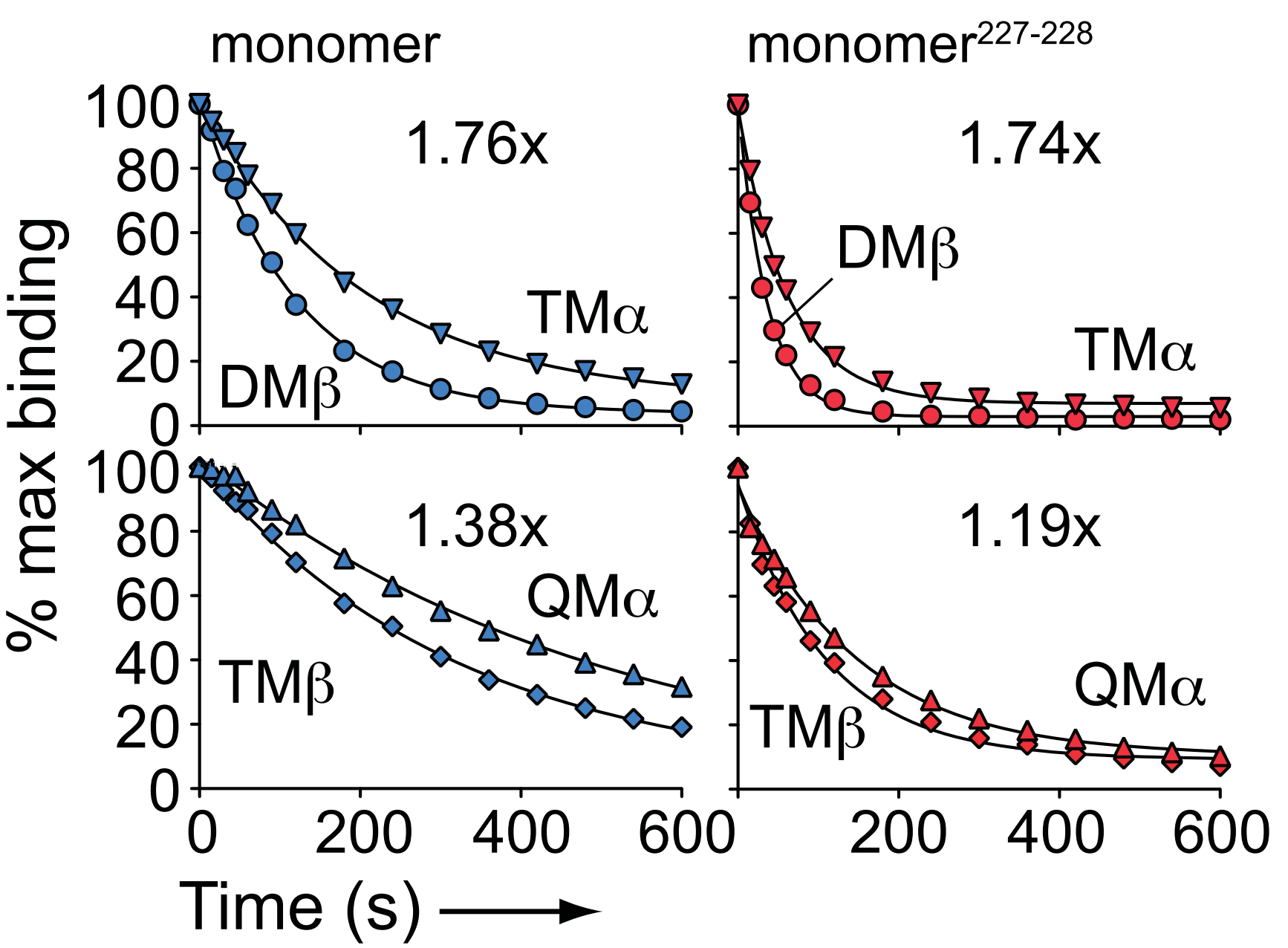
monomer
monomer227-228
1.76x
1.74x
DMβ
TMα
TMα
DMβ
1.38x
1.19x
QMα
QMα
TMβ
TMβ
% max binding
100
80
60
40
20
0
0
200
400
600
200
400
600
Time (s)

-- SUP. FIG.5--